IJIRAE:: International Journal of Innovative Research in Advanced Engineering ISSN: 2349-2163
Volume 13, Issue 02, February 2026 https://www.ijirae.com/archives
https://doi.org/10.26562/ijirae.2026.v1302.02

Impact of Cattaneo-Christov heat flux on MHD flow of Non-Newtonian Fluids over a Stretching Sheet

C.Sulochana
Senior Professor, Department of Mathematics,
Gulbarga University, Kalaburagi, India
Corresponding Author Email Id:math.sulochana@gmail.com
https://orcid.org/0000-0003-1123-5254
Pooja Somashekhar Dashatty
Research Scholar, Dept. of Mathematics,
Gulbarga University, Kalaburagi, Karnataka, India
poojarpatil7974@gmail.com

Publication History
Manuscript Reference No: IJIRAE/RS/Vol.13/Issue02/AEFB26.FBAE10081
Research Article | Open Access | Double-Blind Peer-Reviewed | Article ID: IJIRAE/RS/Vol.13/Issue02/AEFB26.FBAE10081
Received:20,January 2026, Revised: 01, February 2026, Accepted: 09, February2026,Published Online:12,February 2026.
https://www.ijirae.com/volumes/Vol13/iss-02/02.AEFB26.FBAE10081.pdf
Article Citation:Sulochana,Pooja(2026),Impact of Cattaneo-Christov heat flux on MHD flow of Non-Newtonian Fluids over a Stretching Sheet ,IJIRAE: International Journal of Innovative Research in Advanced Engineering, Volume 13, Issue 02 of 2026 pages 76-94 **Doi:>**https://doi.org/10.26562/ijirae.2026.v1302.02
BibTeX Key: Sulochana@2026Impact
IJIRAE papers should be cited as IJIRAE (International Journal of Innovative Research in Advanced Engineering, AM Publications, India 2025, ISSN 2349-2163, https://doi.org/10.26562/ijirae.2026.v1302.02The journal's official abbreviation is IJIRAE.Orcid: https://orcid.org/0009-0004-9398-7488

Abstract: This work examines the influence of Cattaneo–Christov heat flux on magneto hydrodynamic (MHD) flow of non-Newtonian fluids; Jeffrey, Maxwell and Oldroyd-Bover a stretching sheet, integrating activation energy and velocity slip effects. The governing partial differential equations are converted into similarity-based nonlinear ordinary differential equations and solved numerically utilizing MATLAB's BVP5C solver. Results reveal that higher relaxation-to-retardation ratios, larger Deborah numbers and increased slip significantly reduce fluid velocity with Oldroyd-B fluid and Maxwell fluid exhibits the greatest decrease, while Jeffrey fluid is minimally affected. Thermal Deborah number enhances heat flux relaxation, leading to elevated temperature profiles and a thicker thermal boundary layer. Increased activation energy slows chemical reactions but raises nanoparticle concentration with Jeffrey fluid. Validation against previous studies confirms the accuracy and reliability of the solutions. Furthermore, skin friction decreases with magnetic parameters, relaxation ratio and slip, whereas the Nusselt number increases with heat flux relaxation and radiation but diminishes due to Brownian motion, thermophoresis and non-uniform heat. Sherwood number rises with Lewis number, reaction rate, Brownian motion and reaction strength but decreases with thermophoresis and activation energy. Maxwell fluid consistently exhibits the most favourable transport rates, Jeffrey fluid the least, with Oldroyd-B liquid intermediate due to rheological differences.
Keywords: MHD, Non-Newtonian fluids (Jeffrey, Maxwell & Oldroyd-B), Cattaneo-Christov heat flux, Activation energy & Slip effects.

Nomenclature

u, v Velocity components along the x and y axes
D_B Brownian diffusion coefficient
D_T Thermophoresis diffusion coefficient
C Volumetric volume expansion coefficient
k^* Rosseland mean absorption coefficient
K_r^2 Rate of chemical reaction
λ Ratio of relaxation time to the retardation time
λ_1 Relaxation time
λ_2 Retardation time
λ_3 Relaxation time of the heat flux
a Stretching rate
E_a Activation energy

ρ_p Nanoparticles density
θ Dimensionless temperature variable
C_∞ Concentration at ambient
φ Nanoparticle volume fraction
υ Kinematic viscosity
σ^* Stefan-Boltzmann constant
C_w Concentration at wall
α Thermal diffusivity
η Similarity variable
$(\rho c)_f$ Heat capacities of nanofluid
$(\rho c)_p$ Effective heat capacity of the nanoparticles

1. INTRODUCTION

Magneto hydrodynamics (MHD) examines the dynamics of electrically conducting fluids in magnetic fields, where induced currents generate Lorentz forces that influence momentum, thermal & material transport. Utilization in cooling of nuclear reactors, plasma physics, metallurgy, astrophysics & modern energy systems. B. Srisailam et al.[1] noted that the impact of dissipative heating on thermal transport over a porous elongating sheet remains unexplored. Kapilkumar et al.[2]discussed MHD Jeffrey nanofluid flow near a stagnation point across a permeable elongating sheet with heat transfer via radiation, while K.A Khan et al.[3]Explored the effects of thermophoresis & Brownian motion on thermal & material transport in Casson–Williamson & Maxwell nanofluid flows over an elongating sheet. S.Karthik et al.[4]Investigated mass diffusion and radiation impact on thermal & mass transport in MHD Powell–Eyring flow past an absorptive wall.

Non-Newtonian fluids exhibit shear-dependent viscosity, deviating from Newton's law of viscosity, with applications spanning biomedical systems, food processing, polymer engineering and advanced heat transfer technologies. N.Sandeep and C.Sulochana[5]analysed momentum and heat transfer in non-Newtonian fluids over an elongating sheet under the influence of a magnetic field, thermal effects and suction.M.Almakki et al.[6]studied heat transfer and irreversibility in stagnation-point flow of nanofluids based on three non-Newtonian fluids, considering magnetic, Brownian, thermophoretic and slip effects. A.S.Khan et al.[7]investigated unsteady MHD flow of three non-Newtonian fluids past a permeable elongating sheet with variable heating and radiation. P.B.Raafat&F.N.Ibrahim[8]analyzed comparative flow, thermal transport & entropy production of Casson-based binary nanofluids in a parabolic trough solar collector. G. R. Machireddy et al.[9]Investigated the effects of Cattaneo–Christov heat fluxon MHD non-Newtonian fluid flow in Darcy–Forchheimer permeable medium with radiative thermal transfer & non-uniform heating. D.Thenmozhi et al.[10]Examined MHD thermal transport parameters to optimize fluid dynamics in food, ink and lubrication applications.

The Cattaneo–Christov model captures finite-speed heat propagation in non-Newtonian and MHD nanofluid flows, applied to elongating sheet porous media and solar energy systems. T. Hayat et al.[11]Investigated heat transfer and flow of Oldroyd-B fluid past a nonlinear elongating sheet with variable properties, accounting for Cattaneo–Christov heat flux. T.Hayat et al.[12]Studied Darcy–Forchheimer viscoelastic flow past an elongating sheet, considering Cattaneo–Christov heat flux and bulk surface reactions. A.Shahid et al.[13]Investigated non-Fickian thermal and species diffusion in MHD Maxwell flow over a porous elongating sheet, accounting for radiation and chemical reactions. B.M.Shankaralingappa et al.[14]Analyzed Oldroyd-B flow and thermal and species transport over an elongating sheet, considering Cattaneo–Christov diffusion, internal heat generation and absorption, chemical reactions and thermophoresis. F.Shahzad et al.[15]Studied bioconvection in magnetized Burgers nanoliquid flow over an elongating sheet, accounting for Cattaneo–Christov diffusion and the Buongiorno model. P.Sreedevi & P.Sudarsana Reddy [16]investigated fluid flow with heat and species transport in Oldroyd-B SWCNT/MWCNT water hybrid nanofluids over an elongating sheet, accounting for radiation, modified Fourier flux, and convection.A.O.M.Sidahmed et al.[17]examined heat transfer in UCM fluid over an exponentially elongating sheet with chemical reactions, employing the Cattaneo–Christov model. P.Soni et al.[18] investigated 2D MHD Walters' B fluid thermo-fluid transport in a permeable medium, accounting for elastic deformation, non-Fourier heat flux, and viscous dissipation with Newtonian heating.

Nonlinear thermal radiation significantly affects thermal transport & temperature profiles in MHD non-Newtonian nanofluid flows, enhancing accuracy in modeling high-temperature energy & industrial systems. R. Abdullah Mohamed et al.[19]Analyzed MHD non-Newtonian nanofluid flow over an elongating sheet in a permeable medium, considering nonlinear radiative heat transfer and internal thermal generation/absorption. P.Kaswan et al.[20]Employed BP neural networks to model magneto–cross-bioconvective nanofluid flow, accounting for gyrotactic microorganisms and activation energy. K.Mahalakshmi&P.S.R.Murty[21]investigated unsteady MHD mixed convection of TiO□–Al□O□/water hybrid nanofluid in a Darcy porous medium, considering thermal radiation, activation energy, Brownian motion and thermophoresis. Non-uniform heat sources or sinks affect temperature & heat transfer in MHD flows of Jeffrey, Maxwell & Casson nanofluids, with applications in solar energy, industrial processes and thermal management systems. S.Bilal et al.[22] Investigated mixed convection of Jeffrey nanoliquid along an exponentially elongating sheet, accounting for radiation, internal thermal energy generation/absorption, slip and Arrhenius activation energy.

S.Jagadhaetal.[23]examined steady Darcy–Forchheimer Jeffrey nanofluid flow across an variable-thickness elongating sheet with radiation, concentration & magnetic field. Activation energy represents the smallest energy threshold necessary for a chemical reaction. Influencing reaction rates in applications such as combustion, chemical reactors, catalysis & thermal and solutal transport in nanofluid systems. F.Ahmed et al.[24]Investigated MHD Maxwell nanofluid dynamics with Arrhenius-type chemical activation, emphasizing linear &impact of nonlinear radiative heat transfer on the boundary layer. Y.Leng et al.[25]Studied MHD Casson nanofluid flow along a nonlinear elongating sheet in a Darcy–Forchheimer permeable medium with suction/injection,Joule heating,radiation,stratification,activation energy & chemical reactions.

S.A.A.Shah et al.[26]Employed MATLAB's bvp4c to investigate the effects of activation energy and solar radiation on thermal and solutal transport in non-Newtonian Casson, Williamson and Prandtl nanofluid flows for renewable energy applications. S.J.Tao et al.[27]Numerically investigated energy dissipation in magnetized bioconvective flow of micropolar nanofluid over a Darcy–Forchheimer elongating sheet, accounting for combined thermal, chemical and bioconvective effects. K.Sudarmozhi et al.[28]employed MATLAB's bvp4c solver to analyze Maxwell fluid flow over a permeable flat plate, accounting for MHD effects, internal energy generation, radiation, chemical kinetics, activation energy and slip effects.M.V.Krishna and A.G.V.Kumar[29]conducted a numerical investigation of MHD flow in the boundary layer and thermal energy transfer of Jeffrey nanofluid over an elongating sheet, considering temperature jump, velocity slip and variable internal heat generation and absorption.P.Rana and R.Bhargava[30]employed the finite element method to study steady laminar nanofluid flow over a nonlinear elongating sheet, accounting for the effects of thermophoresis and Brownian motion. S.A.Lone et al.[31]Applied the HAM technique to investigate steady laminar MHD Casson fluid flow over a stratified elongating sheet, considering multiple thermal and mass transfer effects. Finally, C.Sulochana et al.[32]investigated magneto-bioconvective Eyring–Powell nanofluid transport over an elongated sheet, accounting for activation energy, nonlinear radiative heat transfer and the effects of motile microorganisms under a magnetic field.

The combined effects of Cattaneo–activation energy, Christov heat flux and velocity slip on Maxwell, Jeffrey and Oldroyd-B fluids over a stretching sheet have received limited attention, despite extensive work on MHD flows of non-Newtonian nanofluids. This research fills that gap by systematically comparing the three viscoelastic models under the same conditions, highlighting differences in velocity, temperature and concentration distributions. Incorporating finite-speed thermal propagation with magnetohydrodynamic effects, the analysis provides a more realistic depiction of high-temperature, electrically conducting fluids. Numerical solutions are obtained via MATLAB's BVP5C solver, yielding new insights into the interplay of viscoelasticity, slip, magnetic fields and activation energy in advanced heat and mass transfer applications.

2. FORMULATION AND SOLUTION OF THE PROBLEM

We have considered a steady, incompressible flow of non-Newtonian fluids (Jeffrey, Maxwell, Oldroyd-B) over horizontally stretching sheet. Flow is confined to $y > 0$, with the sheet stretching is in the x-direction with a velocity $U_w = ax,\ (a > 0)$. A uniform magnetic field B_0 is applied in the transverse direction y normal to the plate. Nanofluid is treated as a thermally equilibrated single-phase fluid, allowing velocity slip between nanoparticles and the base fluid. Surface temperature T_w and nanoparticle concentration C_w are constant, while ambient fluid maintains T_∞ and C_∞. A constant wall temperature has been taken into account in place of a variable heat flux(Figure 1).

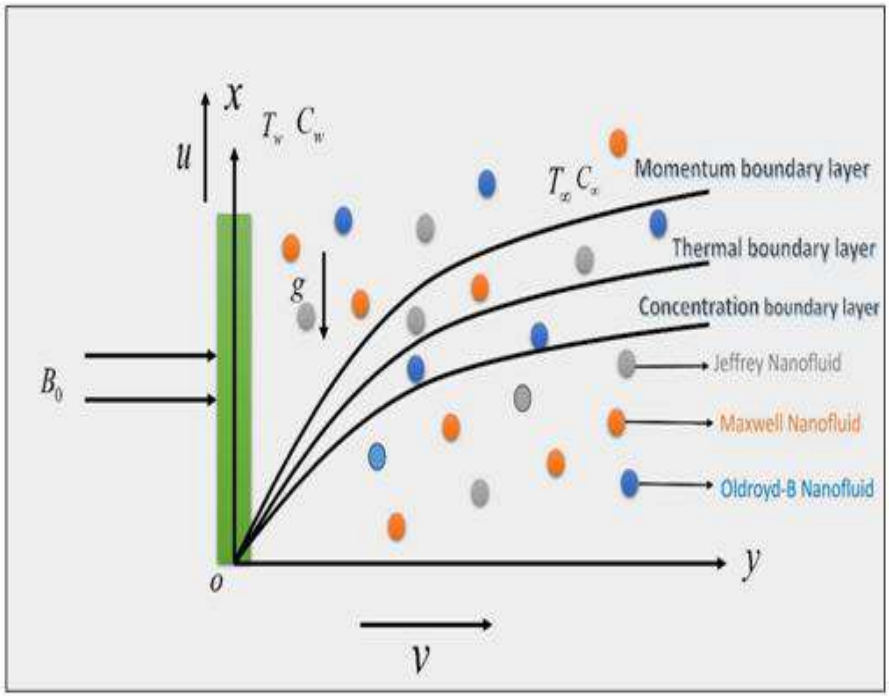

Figure 1: Flow representation of the system

IJIRAE:: International Journal of Innovative Research in Advanced Engineering ISSN: 2349-2163
Volume 13, Issue 02, February 2026 https://www.ijirae.com/archives
https://doi.org/10.26562/ijirae.2026.v1302.02

The boundary layer equations that regulate the two-dimensional flow of Jeffrey, Maxwell and Oldroyd-B fluids, involving continuity, momentum and heat transfer under Cattaneo–Christov heat flux. The concentration equation that incorporates the activation energy, it can be expressed as,

$$u_x + v_y = 0 \quad (1)$$

$$uu_x + vu_y = \frac{\upsilon}{1+\lambda}\left(u_{yy} + \lambda_1\left(uu_{xyy} + vu_{yyy} - u_x u_{yy} + u_y u_{xy}\right)\right) - \frac{\sigma B_0^2}{\rho_f}u - \lambda_2\left(u^2 u_{xx} + 2uvu_{xy} + v^2 u_{yy}\right) \quad (2)$$

$$uT_x + vT_y = \alpha T_{yy} + \frac{\rho_p C_p}{(\rho C)_f}\left(D_B C_y T_y + \frac{D_T}{D_\infty}\left(T_y\right)^2\right) - \frac{1}{(\rho c)_f}\frac{\partial q_r}{\partial y} + \frac{q'''}{(\rho c)_f} - \lambda_3\left(uu_x T_x + vv_y T_y + uv_x T_y + u^2 T_{xx} + vu_y T_x + 2uvT_{xy} + v^2 T_{yy}\right) \quad (3)$$

$$uC_x + vC_y = D_B C_{yy} + \frac{D_T}{D_\infty}T_{yy} - K_r^2\left(\frac{T}{T_\infty}\right)^m \exp\left(\frac{-E_a}{kT}\right)(C - C_\infty) \quad (4)$$

The current investigation involves three distinct non-Newtonian fluid models which are formulated on the basis of these assumptions are,

I. $\lambda = 0,\ \lambda_1 \neq 0,\ \lambda_2 \neq 0$: Oldroyd-B liquid model.

II. $\lambda = 0,\ \lambda_1 = 0,\ \lambda_2 \neq 0$: Maxwell liquid model.

III. $\lambda \neq 0,\ \lambda_1 \neq 0,\ \lambda_2 = 0$: Jeffrey liquid model.

The resulting boundary conditions were given as follows:

$$U = U_W + U_{slip}, v = 0, T = T_w, C = C_w \text{ at } y = 0, \quad (5)$$

$$u = 0, T = T_\infty, C = C_\infty, \text{ as } y \to \infty, \quad (6)$$

In this context, U_{slip} denotes the velocity corresponding to slip at surface, assuming negative values because ofthe stretching effect. The slip formulation utilized here is to accommodate the arbitrary Knudsen number and is written as:

$$U_{slip} = \frac{2}{3}\left(\frac{3-\chi l^3}{\chi} - \frac{3}{2}\frac{1-l^2}{k_n}\right)\omega\frac{\partial u}{\partial y} = \frac{1}{4}\left[l^4 + \frac{2}{k_n^2}(1-l^2)\right]\omega^2\frac{\partial^2 u}{\partial y^2} = A\frac{\partial u}{\partial y} + B\frac{\partial^2 u}{\partial y^2} \quad (7)$$

Let $l = \min\left[\frac{1}{k_N}, 1\right]$, where χ denotes momentum accommodation factor, constrained within $0 \le \chi \le 1$, The symbol ω denotes average distance between molecular collisions, and Knudsen number k_n has been described as"ratio of mean free path to characteristic length scale of flow. Based on this definition, for any specified k_n, the value of l lies within the range $0 \le l \le 1$. Since molecular mean free path is continually positive, it follows that $B < 0$, where A represents strictly a positive constant.

In this context, q''' represents internal energy production or consumption that varies with both position and temperature, characterizing a non-uniform thermal source/sink.It may be formulated as follows:

$$q''' = \left(\frac{kU_w(x)}{xv}\right)\left[A^*\left(T_w - T_\infty\right)f'(\eta) + B^*\left(T - T_\infty\right)\right] \quad (8)$$

Here, T_w and T_∞ represents temperatures at surface and at a point far from surface, respectively. The constants A^* & B^* were coefficients related to position &. Temperature dependent thermal source/sink. It should be noted that positive values of A^* & B^* correspond to internally generated heat sources, whereas non-positive values indicate internally generated heat sinks. In comparison with the linear Rosseland approximation, this study adopts the nonlinear Rosseland diffusion model, which remains valid for low and high values temperature distinctions between T_w & T_∞. Utilizing this nonlinear approach, radiative heat flux is assumed by:

$$q_r = -\frac{4\sigma^*}{3k^*}\frac{\partial T^4}{\partial y} \quad (9)$$

For boundary layer flow over a horizontal flat" surface, equation (9) results in the following result:

IJIRAE:: International Journal of Innovative Research in Advanced Engineering ISSN: 2349-2163
Volume 13, Issue 02, February 2026 https://www.ijirae.com/archives
https://doi.org/10.26562/ijirae.2026.v1302.02

$$q_r = \frac{16\sigma^* T_\infty^3}{3\sigma^*}\frac{\partial T}{\partial y}. \quad (10)$$

By applying equation (10), energy equation (3) transforms into the following form:

$$uT_x + vT_y = \frac{\partial}{\partial y}\left[\left(\alpha + \frac{16\sigma^* T_\infty^3}{3k^*(\rho c)_f}\right)T_y\right] + \frac{\rho_p c_p}{(\rho c)_f}\left[D_B C_y T_y + \frac{D_T}{D_\infty}(T_y)^2\right] + \frac{q'''}{(\rho c)_f} \quad (11)$$
$$-\lambda_3\left(uu_x T_x + vv_y T_y + uv_x T_y + u^2 T_{xx} + vu_y T_x + 2uvT_{xy} + v^2 T_{yy}\right)$$

Here $\alpha = \frac{k}{(\rho c)_f}$, where k denotes the heat conductivity.

The governing equations are converted into ordinary differential equations by employing following similarity transformations:

$$u = axf'(\eta), v = -\sqrt{a\upsilon}\, f(\eta), \eta = \sqrt{\frac{a}{\upsilon}}y,$$
$$T = T_\infty\left(1+(\theta_W - 1)\theta(\eta)\right), \varphi(\eta) = \frac{C - C_\infty}{C_W - C_\infty}. \quad (12)$$

Here, $\theta_W = \frac{T_W}{T_\infty}$ represents the temperature ratio parameter, where $\theta_W > 1$. Upon applying the aforementioned similarity transformations, equation (4) has been inherently satisfied, whereas equations (2), (4), and (11) can be expressed in following forms:

$$f''' + (1+\lambda)\left[ff'' - f'^2\right] + \beta_1\left[f''^2 - ff''''\right] - (1+\lambda)(M)f' \quad (13)$$
$$-(1+\lambda)\beta_2\left(f'''f^2 - 2ff'f''\right) = 0$$

$$\left[1 + Nr\left(1+(\theta_w - 1)\theta\right)^3\theta'\right]' + \Pr\left[f\theta' + Nb\varphi'\theta' + Nt(\theta')^2\right] + A^* f'(\eta) + B^*\theta(\eta) \quad (14)$$
$$-\Pr\beta_3\left(ff'\theta' + f^2\theta''\right) = 0$$

$$\varphi'' + Lef\varphi' + \frac{Nt}{Nb}\theta'' - Cr\varphi Le(1+\delta\theta)^m \exp\left(\frac{-E}{1+\delta\theta}\right) = 0 \quad (15)$$

The governing boundary conditions were stated as

$$f(0) = 0, f'(0) = 1 + A_1 f''(0) + A_2 f'''(0), \theta(0) = 1, \varphi(0) = 1 \text{ at } \eta = 0, \quad (16)$$
$$f'(\eta) = f''(\eta) = \theta(\eta) = \varphi(\eta) = 0 \text{ as } \eta \to 0. \quad (17)$$

Here, A_1 represents first-order velocity slip parameter, defined as $0 < A_1 = A\sqrt{\frac{a}{\upsilon}}$ and A_2 denotes second-order velocity slip parameter, given by $0 > A_2 = \frac{Ba}{\upsilon}$. Moreover f, θ and φ are functions of η and the prime symbol indicates differentiation with respect to η. The associated parameters are defined as follows:

$\beta_1 = \lambda_1 a$ is Deborah number in regard to relaxation time, $M = \frac{\sigma B_0^2}{\rho f_a}$ is Magnetic parameter, $\beta_2 = \lambda_2 a$ is Deborah number with retardation time, $Nr = \frac{16\sigma^* T_\infty^3}{3kk^*}$ represents Radiation parameter, $Nb = \frac{\tau D_B(C_W - C_\infty)}{\upsilon}$ denotes Brownian motion parameter, $Nt = \frac{\tau D_\tau(T_W - T_\infty)}{\upsilon T_\infty}$ implies Thermophoresis parameter, $\Pr = \frac{\upsilon}{\alpha}$ is Prandtl number, $\beta_3 = \lambda_3 a$ is Deborah number with regard to relaxation time of heat flux, $Le = \frac{\upsilon}{D_B}$ implies Lewis number, $E = \frac{E_a}{k_2 T_\infty}$ denotes Dimensionless activation energy $\delta = \frac{(T_w - T_\infty)}{T_\infty}$ represents Temperature relative parameter and $Cr = \frac{K_r^2}{a}$ is chemical reaction factor.

The Nusselt number (Nu_x), skin-friction coefficient (Cf_x) and Sherwood number (Sh_x) are well-defined as:

IJIRAE:: International Journal of Innovative Research in Advanced Engineering ISSN: 2349-2163
Volume 13, Issue 02, February 2026 https://www.ijirae.com/archives
https://doi.org/10.26562/ijirae.2026.v1302.02

$$Cf_x = \frac{\tau_w}{\rho U_w^2}, Nu_x = \frac{xq_w}{k(T_W - T_\infty)} \& Sh_x = \frac{xq_m}{k(C_W - C_\infty)} \quad (18)$$

Surface heat flux (q_w), surface mass flux (q_m) and shear stress at stretching surface(τ_w) are all" expressed as follows:

$$\tau_w = \frac{\mu}{1+\lambda}\left[\left(u_y\right) + \lambda_1\left(u_{xy} + uy_{xx} + vu_{yy}\right)\right]_{y=0}$$

$$q_w = -kT_y + \left(q_r\right)_w,\ q_m = -D_B C_y \text{ at } y = 0 \quad (19)$$

By substituting expressions for τ_w, q_w & q_m into Equation (21), we obtain:

$$\sqrt{\mathrm{Re}}Cf_x = \left[\frac{1}{1+\lambda}\left(f''(0) + \beta_1\left(f'(0)f''(0)\right) - f(0)f'''(0)\right)\right],$$

$$\frac{Nu_x}{\sqrt{\mathrm{Re}_x}} = -\left(1 + Nr\theta_w^3\right)\theta'(0), \frac{Sh_x}{\sqrt{\mathrm{Re}_x}} = -\varphi'(0), \quad (20)$$

Here $\mathrm{Re}_x = \frac{ax^2}{\upsilon}$ denotes Reynolds number based on local flow conditions.

3. NUMERICAL METHOD INTERPRETATION OF THE FLUID FLOW

The nonlinear differential equations (13)–(15), together with the boundary conditions specified in equations (16)–(17), are solved using Runge–Kutta–Fehlberg (RKF) numerical scheme along with shooting technique. For simplification, the higher-order system is converted into set of first-order differential equations through introduction of following variable substitutions:

$$\left.\begin{array}{lllll} F_1 = f & , F_2 = f' & , F_3 = f'' & , F_4 = f''' & , F_5 = \theta \\ F_6 = \theta' & , F_7 = \phi & , F_8 = \phi' & & \end{array}\right\} \quad (21)$$

With these variables defined, the system can now be formulated as the following set of first-order differential equations:

$$\begin{aligned} F_1' &= F_2 \\ F_2' &= F_3 \\ F_3' &= F_4 \\ F_4' &= \frac{\left(\mathrm{F}_4 + (1+\lambda)\left(\mathrm{F}_1\mathrm{F}_3 - \mathrm{F}_2\mathrm{F}_2\right) + \left(\beta_1\mathrm{F}_3\mathrm{F}_3\right) - (1+\lambda)\mathrm{MF}_2 - (1+\lambda)\beta_2\left(F_4F_1F_1 - 2F_1F_2F_3\right)\right)}{\beta_1\mathrm{F}_1} \\ F_5' &= F_6 \\ F_6' &= \frac{\left(-Pr\left(F_1F_6 + NbF_8F_6 + NtF_6F_6\right) - A^*F_2 - B^*F + \mathrm{Pr}\,\beta_3\left(F_1F_2F_6\right)\right)}{\left(1 + Nr\left(1 + (Tw-1)F_5\right)^3\right) - F_1F_1\,\mathrm{Pr}\,\beta_3} \\ F_7' &= F_8 \\ F_8' &= -LeF_1F_8 - (Nt/Nb)F_6' + CrF_7Le(1+(\delta F_5))^m exp(-E/(1+(\delta F_5))) \end{aligned} \quad (22)$$

The applicable boundary conditions are formulated as:

$$\left.\begin{array}{llll} \mathrm{F}_1(0)\text{-}0 & , \mathrm{F}_2(0)\text{-}(1+\mathrm{A1}^*F_3(0)+\mathrm{A2}^*\mathrm{F}_4(0)) & , \mathrm{F}_5(0)\text{-}1 & ,\mathrm{F}_7(0)\text{-}1 \\ \mathrm{F}_2(\infty)\text{-}0 & , \mathrm{F}_3(\infty)\text{-}0 & , \mathrm{F}_5(\infty)\text{-}0 & ,\mathrm{F}_7(\infty)\text{-}0 \end{array}\right\} \quad (23)$$

Finally, the set of ordinary differential equations (21)–(22) together with boundary conditions given in equation (23) is reduced by approximating the unknown boundary values. The corresponding initial value problem is subsequently computed numerically through the MATLAB BVP5C solver over the specified domain of interest.

4. VALIDATION OF THE RESULT

Table 1 determines the validation of current findings, where influence of the Prandtl number under different physical parameters is examined. The numerical accuracy of the Matlab-based solutions is confirmed by comparing our results with those of M. Veer Krishna [29], after ignoring a few parameters. The close agreement between both results validates the accuracy of the current solutions.

Further more, **Table 1** ensures that the developed Matlab-based BVP5C numerical code is reliable and produces reasonable results within the considered region. Therefore, it is considered that the validation provided in Table 1 is adequate for confirming reliability of current similarity solutions.

Table 1: Comparison table for $-\theta'(0)$ with

Pr	M.Veer Krishna [29]	Present Result
2	0.911352755774	0.872927162
7	1.895400395478	1.858791369
20	3.353901838744	3.486376734

$$\beta_1 = \lambda = A_1 = Nr = 0.5,\ \beta_2 = \beta_3 = \delta = E = 0, m = 1, Nb = Nt = 10^{-6},\ A^* = B^* = Cr = 0.1, M = 0.3,$$
$$A_2 = -1, \theta_w = 1.2,\ Le = 10, \Pr = 6.2.$$

5. RESULTS AND DISCUSSION

The behaviour under the dynamically regulated parameter is (M), (λ), (A_1), (A_2), (β_1), (β_2), (Nr), (θ_w), (Pr), (Nb), (Nt), (A^*), (B^*), (β_3), (Le), (Cr), (δ) & (E). Figures 2–21 present the analysis of the dimensionless velocity, temperature, as well as concentration distributions for 3 distinct non-Newtonian fluids.

The values of the flow parameters are constrained for numerical evaluation, such as $Nb = Nt = A^* = B^* = Cr = 0.1$, $E = \delta = 0.2$, $M = 0.3$, $A_2 = -1$, $\theta_w = 1.2$, $Le = 10, \Pr = 6.2$ & $\beta_1 = \beta_2 = \beta_3 = Nr = A_1 = \lambda = m = 0.5$. The variation of velocity profile under different physical parameters is illustrated in Figures 2–7 and the related discussion is outlined as follows.

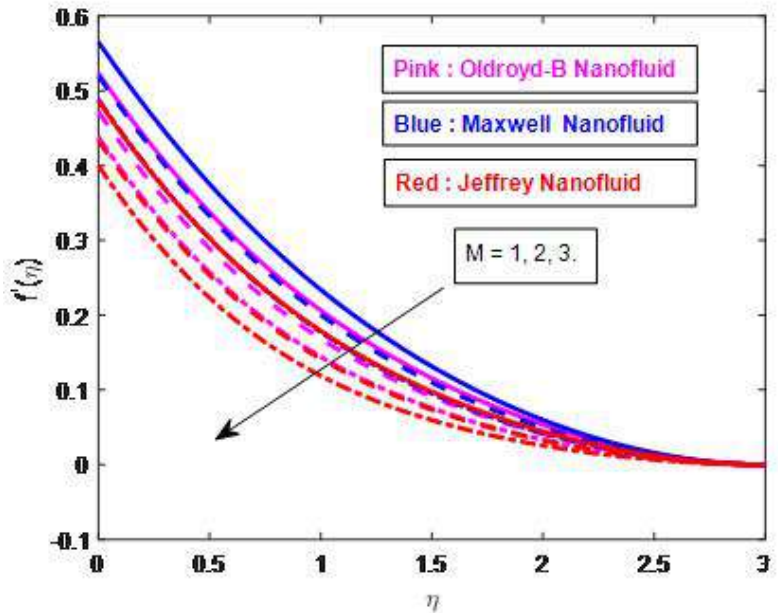

Figure 2: Impression of M on $f'(\eta)$

Figure 2 shows that enhancing M strengthens the Lorentz force, which reduces $f'(\eta)$ in three non-Newtonian fluids among them, Maxwell fluids exhibit the greatest flow suppression, Jeffrey fluids maintain the highest velocities and thermal relaxation effects capture realistic thermal magnetic interactions.**Figure 3** shows that increasing λ reduces $f'(\eta)$ in the three non-Newtonian fluids, with Oldroyd-B showing strongest damping and Jeffrey the weakest, emphasizing the role of relaxation retardation balance in flow resistance and the Cattaneo Christov model in enhancing heat-related magnetic coupling for better heat transfer and flow control. **Figure 4** shows that as A_1 increases, $f'(\eta)$ decreases for all three non-Newtonian fluids, with Maxwell exhibiting the greatest sensitivity and Jeffrey the least, a behaviour shaped by relaxation retardation effects.**Figure 5** shows that decreasing A_2 reduces $f'(\eta)$ for all three non-Newtonian fluids due to weakened fluid–surface interaction, with Maxwell being most & Jeffrey least sensitive, governed by relaxation–retardation effects in the MHD boundary layer. **Figure 6** shows that increasing β_1 decreases $f'(\eta)$ for all three non-Newtonian fluids, due to stronger elastic resistance and reduced momentum transfer, with the Maxwell fluid being most affected and the Jeffrey fluid least affected, reflecting the role of relaxation–retardation interplay in suppressing MHD flow.

IJIRAE:: International Journal of Innovative Research in Advanced Engineering ISSN: 2349-2163
Volume 13, Issue 02, February 2026 https://www.ijirae.com/archives
https://doi.org/10.26562/ijirae.2026.v1302.02

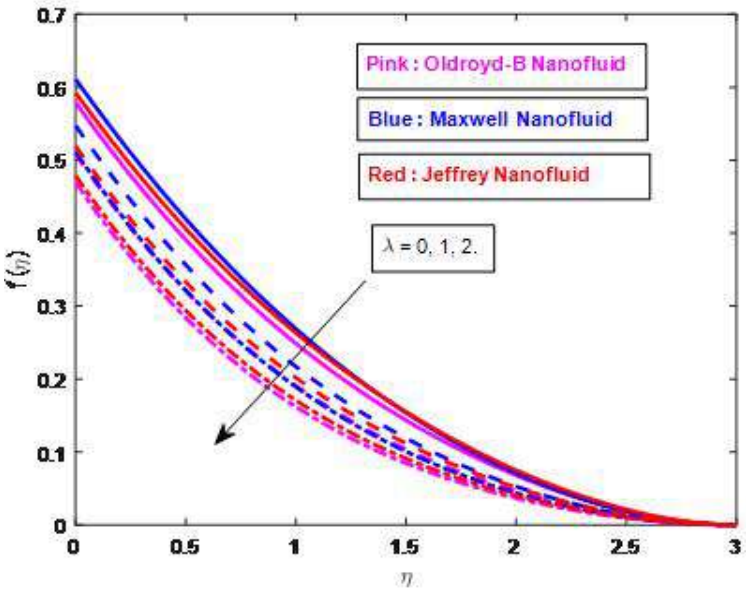

Figure 3: Impression of λ on $f'(\eta)$

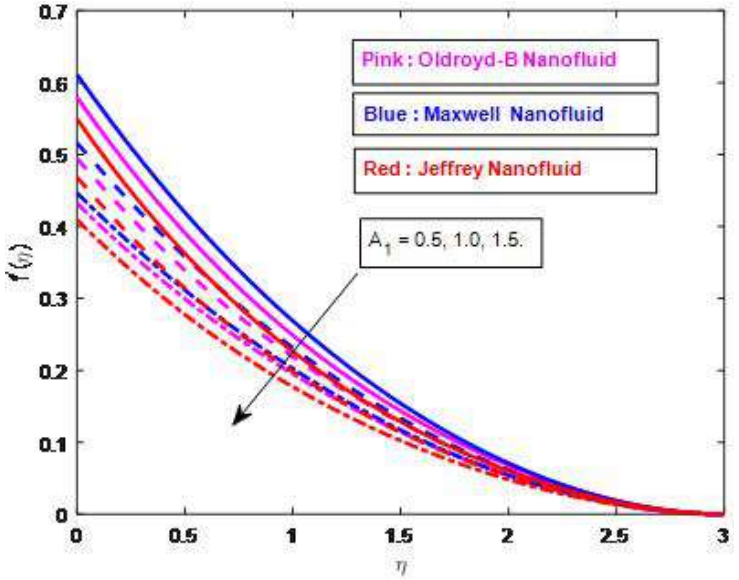

Figure 4: Impression of A_1 on $f'(\eta)$

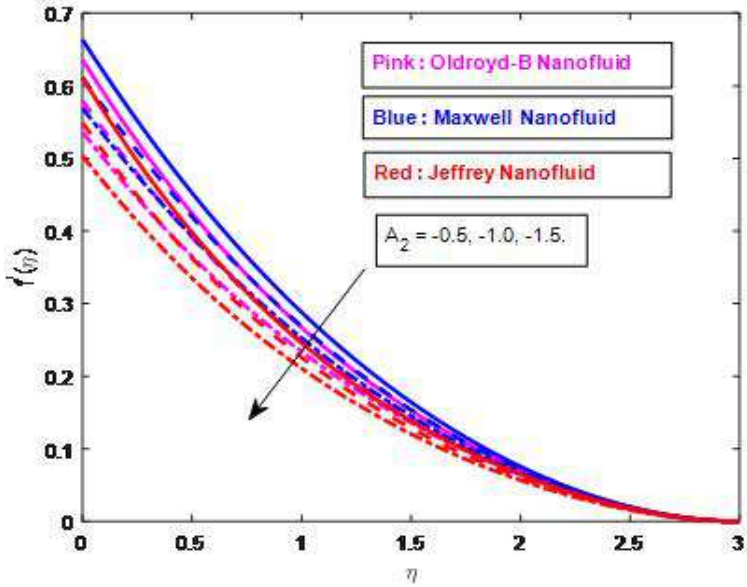

Figure 5: Impression of A_2 on $f'(\eta)$

IJIRAE:: International Journal of Innovative Research in Advanced Engineering ISSN: 2349-2163
Volume 13, Issue 02, February 2026 https://www.ijirae.com/archives
https://doi.org/10.26562/ijirae.2026.v1302.02

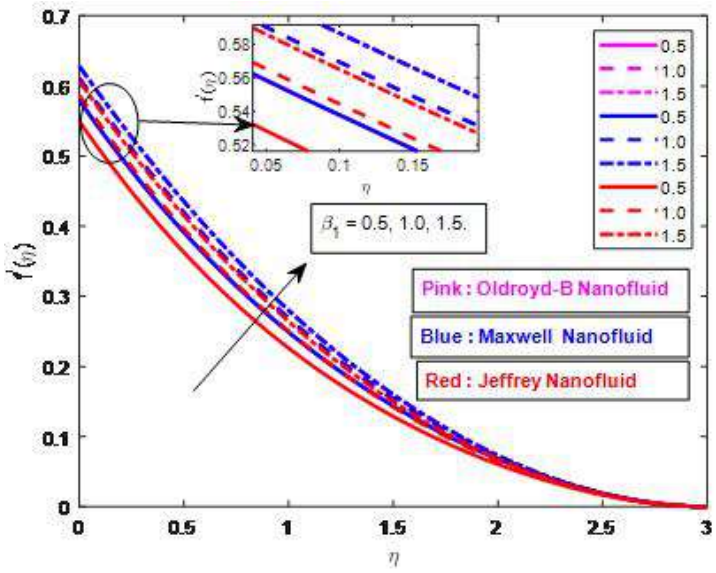

Figure 6: Impression of β_1 on $f'(\eta)$

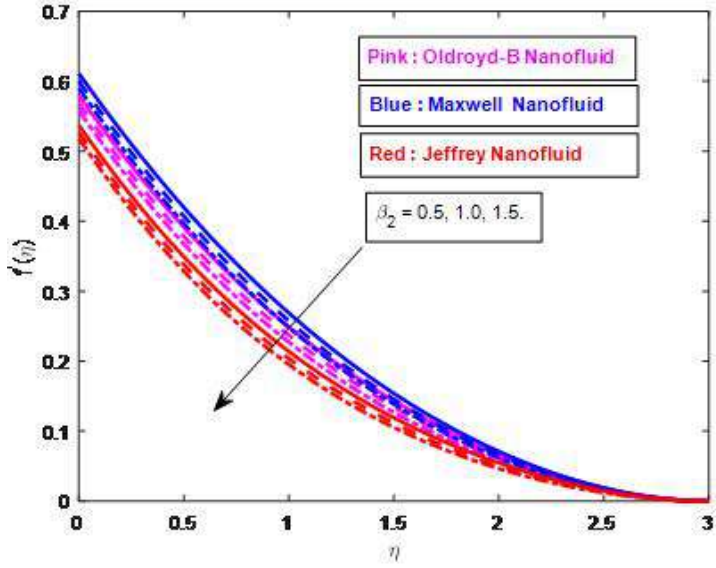

Figure 7: Impression of β_2 on $f'(\eta)$

Figure 7 shows that increasing β_2 reduces $f'(\eta)$ for all three non-Newtonian fluids due to stronger elastic resistance, with the Maxwell fluid having the highest and the Jeffrey fluid the lowest velocity, highlighting the impact of relaxation–retardation & magnetic damping on flow & heat transport.The variation of temperature profile under different physical parameters is illustrated in Figures 8–15 and the related discussion is outlined as follows.

Figure 8 shows that increasing Nr raises $\theta(\eta)$ for all three non-Newtonian fluids by enhancing energy transport, with the Jeffrey fluid having the highest and the Maxwell fluid the lowest temperatures, reflecting the combined effects of relaxationretardation, magnetic damping & radiative heat transfer on MHD thermal performance. **Figure 9** shows that increasing θ_w raises $\theta(\eta)$ considering all three non-Newtonian fluids by boosting the thermal gradient and thickening the boundary layer, with the Jeffrey fluid having the highest and the Maxwell fluid the lowest temperatures, reflecting the mutual effects of relaxation retardation, magnetic damping and non-Newtonian properties on MHD thermal performance.

Figure 10 shows that increasing $\Pr$ decreases $\theta(\eta)$ considering all three non-Newtonian fluids by reducing thermal diffusivity and thinning the thermal layer, with Jeffrey exhibiting the highest and Maxwell the lowest profiles due to relaxation–retardation effects, magnetic damping and non-Newtonian behaviour.**Figure 11** shows that raising Nb increases $\theta(\eta)$ for all three non-Newtonian fluids by boosting nanoparticle driven thermal transport and thickening the thermal layer, with Jeffrey exhibiting the highest and Maxwell the lowest profiles due to relaxation retardation effects, magnetic damping and non-Newtonian behaviour.

IJIRAE:: International Journal of Innovative Research in Advanced Engineering ISSN: 2349-2163
Volume 13, Issue 02, February 2026 https://www.ijirae.com/archives
https://doi.org/10.26562/ijirae.2026.v1302.02

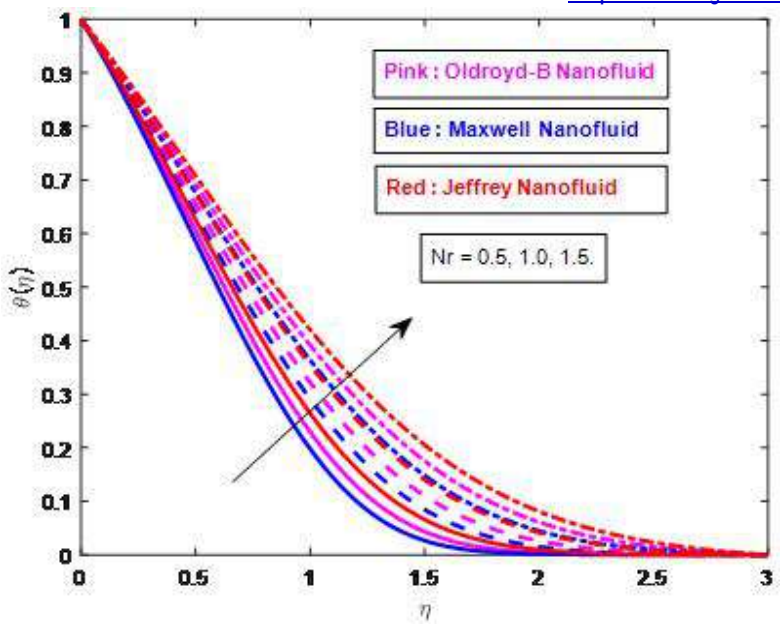

Figure 8: Impression of Nr on $\theta(\eta)$

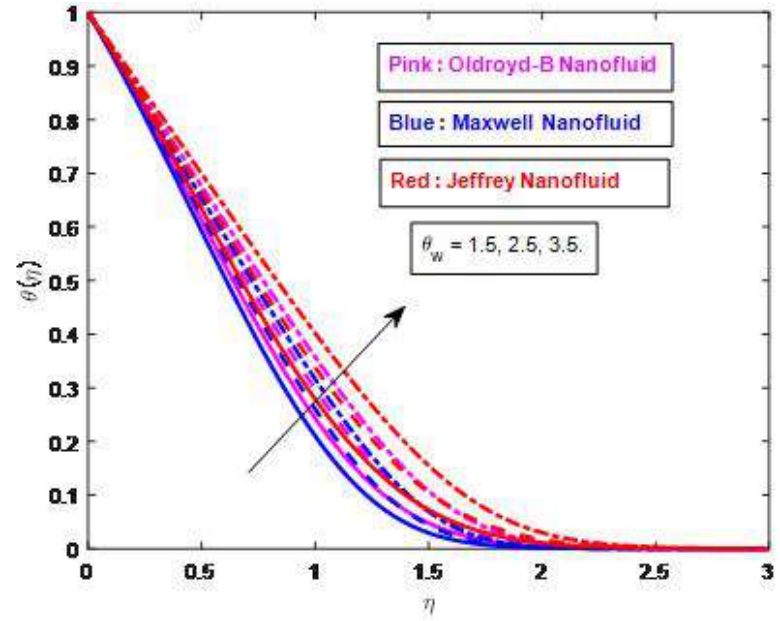

Figure 9: Impression of θ_w on $\theta(\eta)$

Figure 12 indicates that increasing Nt raises $\theta(\eta)$ for all three non-Newtonian fluids by promoting nanoparticle migration from warmer to cooler zones, which enlarges the thermal boundary layer & enhances warmth retention, with Jeffrey showing the highest, Oldroyd-B an intermediate and Maxwell the lowest profiles due to varying elastic resistance to thermal diffusion.

Figure 13 shows that increasing A^* elevates $\theta(\eta)$ considering all three non-Newtonian fluids by enhancing heat energy within the boundary layer, with Jeffrey exhibiting the highest and Maxwell the lowest profiles due to differences in elastic resistance to heat diffusion.**Figure 14** shows that increasing B^* raises $\theta(\eta)$ for all three non-Newtonian fluids by boosting thermal energy and boundary layer thickness, with Jeffrey exhibiting the highest and Maxwell the lowest profiles and the effect being strongest near the wall.

IJIRAE:: International Journal of Innovative Research in Advanced Engineering ISSN: 2349-2163
Volume 13, Issue 02, February 2026 https://www.ijirae.com/archives
https://doi.org/10.26562/ijirae.2026.v1302.02

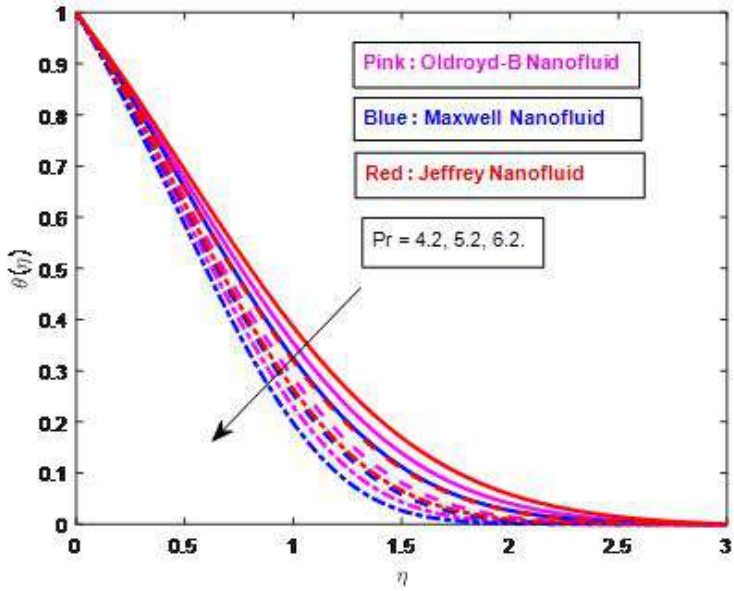

Figure 10 Impression of $\Pr$ on $\theta(\eta)$

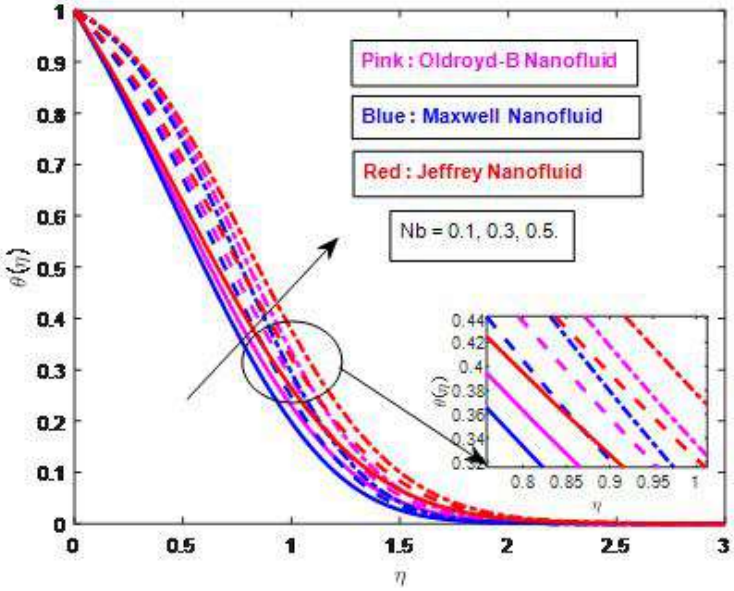

Figure 11: Impression of Nb on $\theta(\eta)$

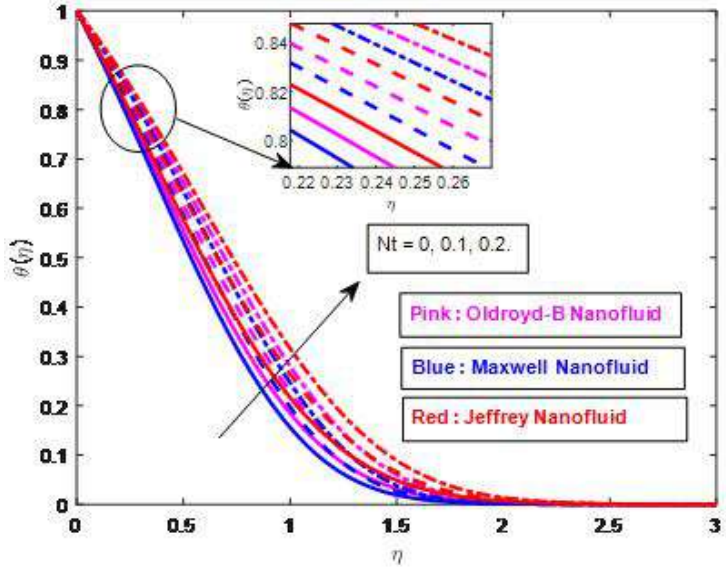

Figure 12: Impression of Nt on $\theta(\eta)$

IJIRAE:: International Journal of Innovative Research in Advanced Engineering ISSN: 2349-2163
Volume 13, Issue 02, February 2026 https://www.ijirae.com/archives
https://doi.org/10.26562/ijirae.2026.v1302.02

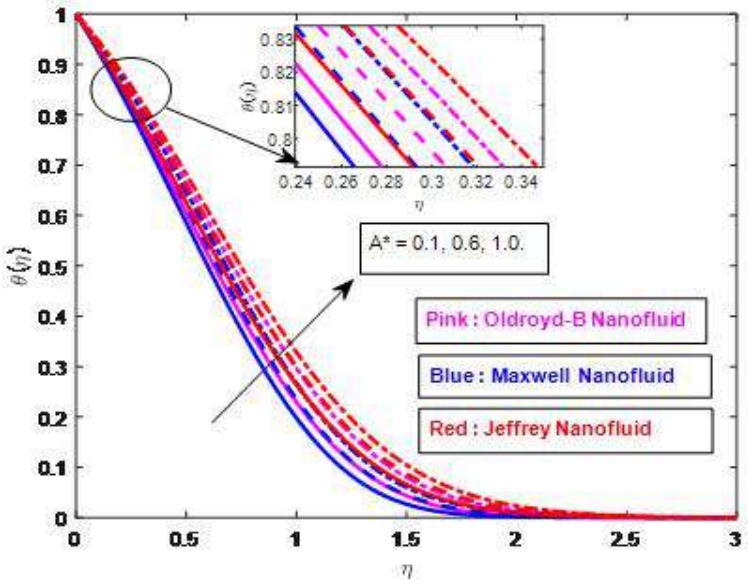

Figure 13: Impression of A^* on $\theta(\eta)$

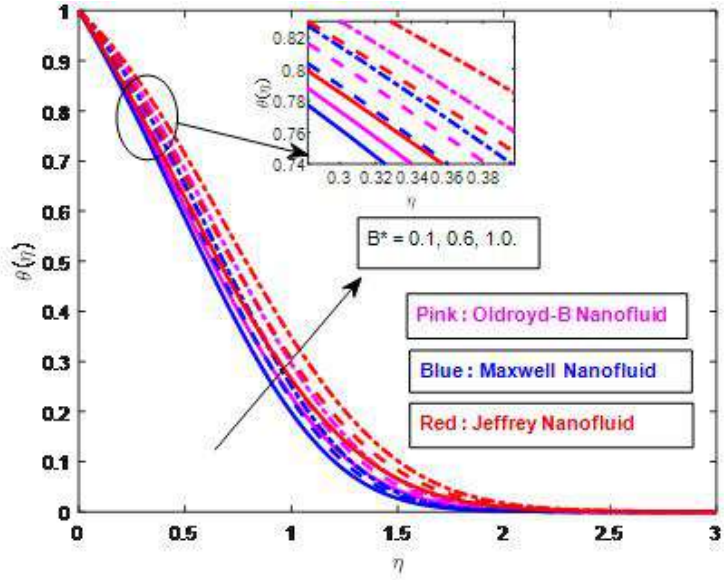

Figure 14: Impression of B^* on $\theta(\eta)$

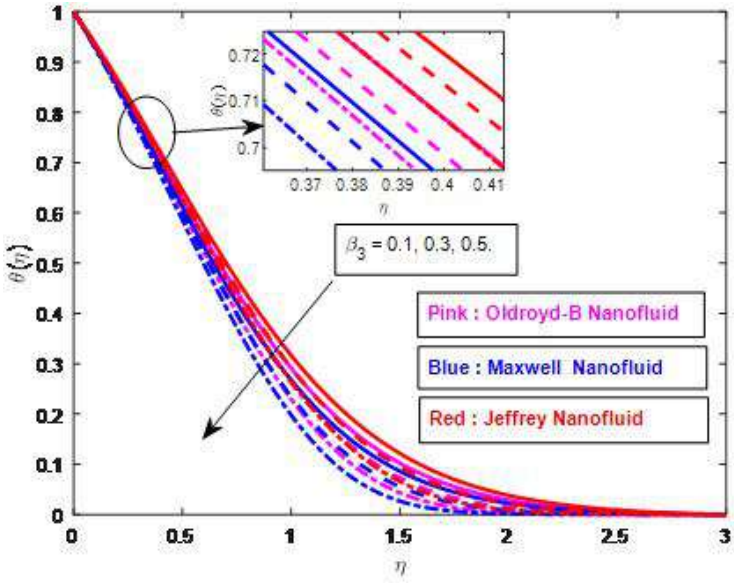

Figure 15: Impression of β_3 on $\theta(\eta)$

Figure 15 shows that increasing β_3 raises $\theta(\eta)$ for all three non-Newtonian fluids by extending heat flux relaxation time, slowing the thermal response & expanding the boundary layer with Jeffrey exhibiting the highest and Maxwell the lowest profiles and the effect being strongest near the wall. The variation of concentration profile under different physical parameters is illustrated in Figures 16–21 and the related discussion is outlined as follows

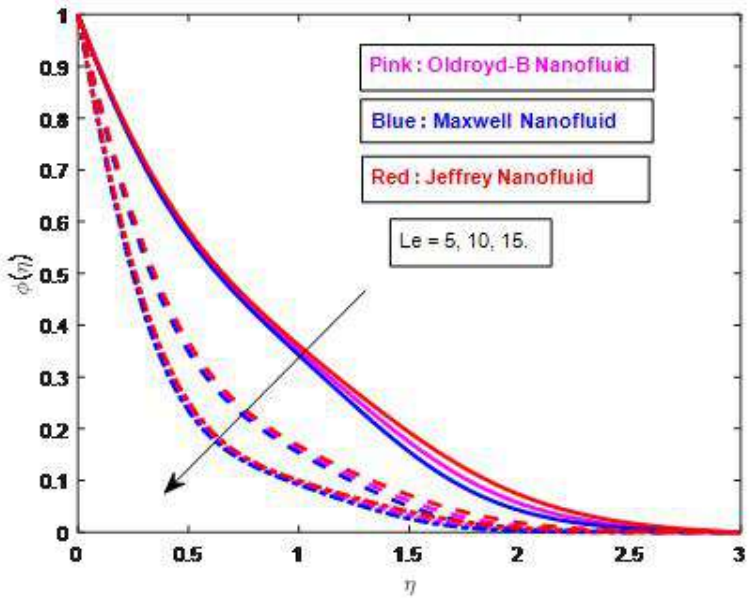

Figure 16: Impression of Le on $\phi(\eta)$

Figure 16 shows that increasing Le reduces $\phi(\eta)$ for all three non-Newtonian fluids by boosting mass diffusion and thinning the concentration boundary layer, with Jeffrey exhibiting the highest and Maxwell the lowest profiles due to differences in elastic resistance. **Figure 17**shows that increasing Nt raises $\phi(\eta)$ considering all three non-Newtonian fluids by enhancing thermophoretic transport from warmer to colder areas and thickening solutal boundary layer, with the strongest effect near the wall and magnitude highest for Jeffrey, lowest for Maxwell and intermediate for Oldroyd-B due to differences in elastic resistance.

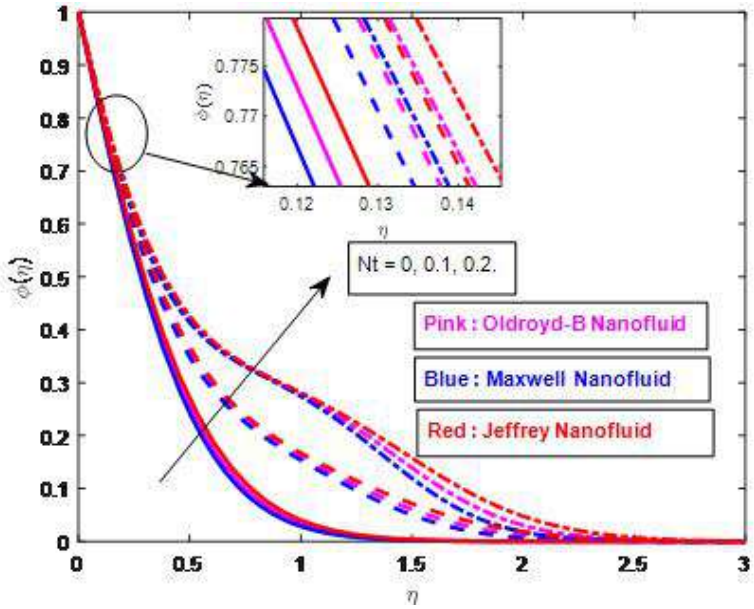

Figure 17: Impression of Nt on $\phi(\eta)$

IJIRAE:: International Journal of Innovative Research in Advanced Engineering ISSN: 2349-2163
Volume 13, Issue 02, February 2026 https://www.ijirae.com/archives
https://doi.org/10.26562/ijirae.2026.v1302.02

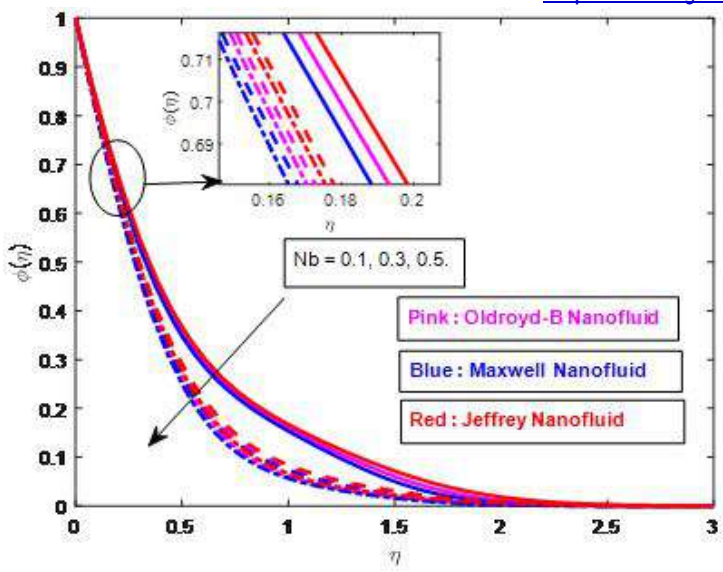

Figure 18: Impression of Nb on $\phi(\eta)$

Figure 18indicates that increasing Nb raises $\phi(\eta)$ for all three non-Newtonianfluids by enhancing Brownian diffusion, with the strongest effect near the wall and magnitude highest for Jeffrey, lowest for Maxwell and intermediate for Oldroyd-B due to differences in elastic resistance.

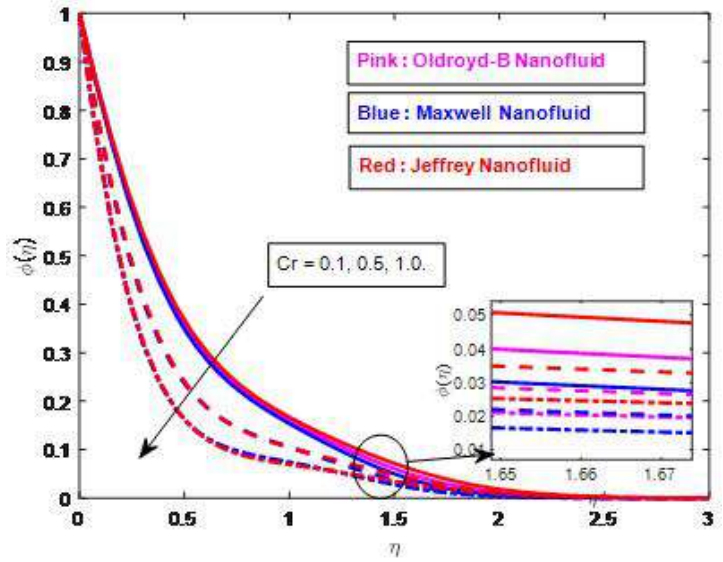

Figure 19: Impression of Cr on $\phi(\eta)$

Figure 19 shows that increasing Cr reduces $\phi(\eta)$ for all three non-Newtonian fluids by accelerating nanoparticle consumption and thinning the concentration layer, with suppression strongest near the wall & concentration highest for Jeffrey, lowest for Maxwell & intermediate for Oldroyd-B due to elastic resistance differences.

Figure 20 shows that increasing δ raises $\phi(\eta)$ considering all three non-Newtonian fluids by strengthening thermophoretic forces that displace nanoparticles from the heated surface, thickening the concentration layermost near the wall with Jeffrey showing the highest, Maxwell the lowest and Oldroyd-B intermediate due to elastic resistance differences.**Figure 21** shows that increasing E elevates $\phi(\eta)$ for all three non-Newtonian fluids by slowing chemical reactions and thickening the concentration boundary layer, with Jeffrey exhibiting the highest, Maxwell the lowest and Oldroyd-B an intermediate profile due to differences in elastic resistance to mass diffusion.

IJIRAE:: International Journal of Innovative Research in Advanced Engineering ISSN: 2349-2163
Volume 13, Issue 02, February 2026 https://www.ijirae.com/archives
https://doi.org/10.26562/ijirae.2026.v1302.02

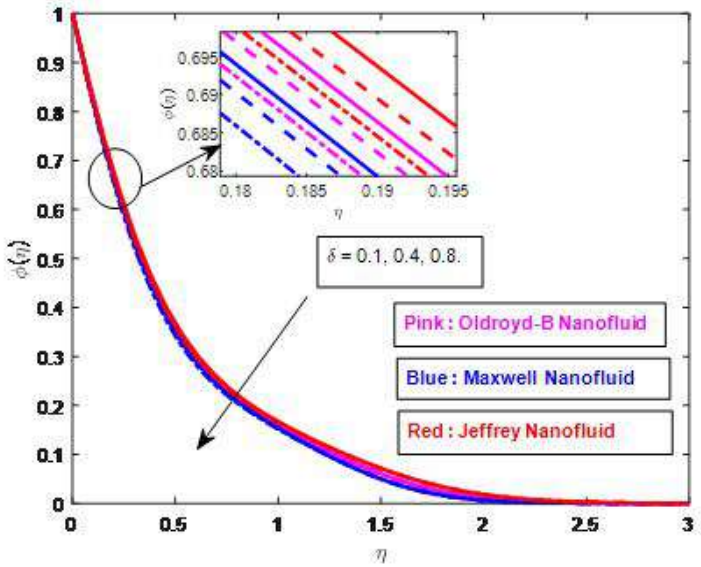

Figure 20: Impression of δ on $\phi(\eta)$

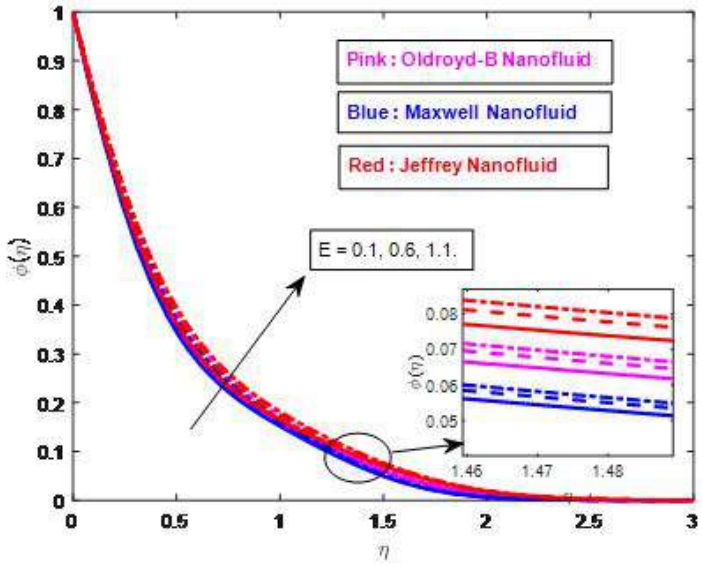

Figure 21: Impression of E on $\phi(\eta)$

Table 2 indicates that the Cf_x in Oldroyd-B, Maxwell and Jeffrey nanofluids is increases in M, λ, A_1 and A_2 lower skin friction, with β_1 producing a strong reduction and β_2 only a mild one, confirming the dominance of relaxation effects. Across all cases, Maxwell exhibits the lowest skin friction, Oldroyd-B remains moderate and Jeffrey records the highest, reflecting their rheological differences.

Table 3 indicates that the Nu_x in Oldroyd-B, Maxwell and Jeffrey fluids rises with larger β_3, Nr, $\Pr$ and θ_w but reduces with larger Nb, Nt, A^* & B^*. Maxwell fluid achieves the greatest heat transfer, Oldroyd-B lies in between and Jeffrey fluid records the lowest. Overall, nonlinear radiation and heat flux relaxation act as the main enhancers of conduction, while nanoparticle effects and non-uniform heating suppress it.

Table 4 indicates that the Sh_x for Oldroyd-B, Maxwell and Jeffrey nanofluids increases with Le, Nb, Cr and δ but decreases with Nt and E. The Maxwell fluid shows the highest values, Oldroyd-B lies in between and Jeffrey records the lowest due to viscoelastic effects.

IJIRAE:: International Journal of Innovative Research in Advanced Engineering ISSN: 2349-2163
Volume 13, Issue 02, February 2026 https://www.ijirae.com/archives
https://doi.org/10.26562/ijirae.2026.v1302.02

Table 2: Effect of M , λ , A_1, A_2 , β_1 & β_2 on Cf_x .

M	λ	A_1	A_2	β_1	β_2	Cf_x		
0.5	0.5	0.5	-1	0.5	0.5	Oldroyd-B	Maxwell	Jeffrey
1.0						-0.54907	-0.67797	-0.36397
2.0						-0.54474	-0.66686	-0.35942
3.0						-0.54002	-0.65754	-0.35499
	0.0					-0.55117	-0.68724	-0.54579
	1.0					-0.27666	-0.33992	-0.27511
	2.0					-0.18349	-0.22393	-0.18281
		0.5				-0.55117	-0.68724	-0.36640
		1.0				-0.43552	-0.52990	-0.29011
		1.5				-0.35976	-0.42915	-0.23982
			-0.5			-0.63669	-0.78461	-0.43062
			-1.0			-0.55117	-0.68724	-0.36640
			-1.5			-0.49056	-0.61492	-0.32209
				0.5		-0.55117	-0.55117	-0.36640
				1.0		-0.68724	-0.68724	-0.45439
				1.5		-0.82716	-0.82716	-0.54571
					0.5	-0.55117	-0.68724	-0.36905
					1.0	-0.55514	-0.68947	-0.37096
					1.5	-0.55815	-0.69095	-0.37237

Table 3: Effect of Nr , θ_w, $\Pr$, Nb , Nt , A^* , B^* & β_3 on Nu_x .

Nr	θ_w	$\Pr$	Nb	Nt	A^*	B^*	β_3	Nu_x		
0.5	1.2	6.2	0.1	0.1	0.1	0.1	0.5	Oldroyd-B	Maxwell	Jeffrey
0.5								1.24961	1.30842	1.18791
1.0								1.68613	1.77008	1.59841
1.5								2.03810	2.13819	1.93569
	1.5							1.85539	1.94655	1.75964
	2.5							6.06269	6.40956	5.69534
	3.5							14.3270	15.2799	13.3093
		4.2						1.07824	1.13327	1.02114
		5.2						1.17756	1.23554	1.11659
		6.2						1.24961	1.30842	1.18791
			0.1					1.24961	1.30842	1.18791
			0.3					0.71435	0.74901	0.67759
			0.5					0.39178	0.41133	0.37079
				0.0				1.48846	1.55939	1.41446
				0.1				1.24961	1.30842	1.18791
				0.2				1.05206	1.10060	1.00078
					0.1			1.24961	1.30842	1.18791
					0.6			1.08361	1.13429	1.03119
					1.0			0.95056	0.99471	0.90562
						0.1		1.24961	1.30842	1.18791
						0.6		1.01616	1.08846	0.93764
						1.0		0.80901	0.89616	0.71070
							0.1	1.19852	1.25018	1.14433
							0.3	1.22271	1.27812	1.16458
							0.5	1.24961	1.30842	1.18791

Table 4: Effect of Le, Nb, Nt, Cr, δ & E on Sh_x.

Le	Nb	Nt	Cr	δ	E	Sh_x		
10	0.1	0.1	0.1	0.2	0.2	Oldroyd-B	Maxwell	Jeffrey
5.0						1.12482	1.14992	1.09944
10						1.85913	1.90515	1.81267
15						2.39129	2.45065	2.33185
	0.1					1.85913	1.90515	1.81267
	0.3					2.00867	2.06192	1.95504
	0.5					2.02036	2.07419	1.96617
		0.0				1.98165	2.03377	1.92935
		0.1				1.85913	1.90515	1.81267
		0.2				1.85479	1.90170	1.80715
			0.1			1.85913	1.90515	1.81267
			0.5			2.75002	2.77952	2.72113
			1.0			3.54901	3.57357	3.52485
				0.1		1.84703	1.89345	1.80012
				0.4		1.88179	1.92708	1.83616
				0.8		1.92229	1.96629	1.87808
					0.1	1.88393	1.92923	1.83829
					0.6	1.77679	1.82539	1.72740
					1.1	1.70435	1.75544	1.65210

6. CONCLUSIONS

In this investigation, the impact "of Cattaneo-Christov heat flux on the MHD flow of non-Newtonian fluids over a stretching sheet is examined. The non-Newtonian fluids (Jeffrey Maxwell & Oldroyd-B), composed of MHD, Activation energy & Slip effects**.** The following major results are found out during these investigations,

- Increasing the ratio of relaxation to retardation time, Deborah" numbers & slip parameters significantly reduced velocity in all three non-Newtonian fluids, with Oldroyd-B and Maxwell fluids showing the strongest reductions and Jeffrey the weakest.
- The thermal Deborah number extended heat flux relaxation, which raised temperature and thickened the thermal boundary layer, while higher activation energy elevated concentration by slowing reaction rates, with Jeffrey fluid consistently showing the highest profiles.
- Validation with Veer Krishna [29] confirmed that the present MATLAB-based BVP5C solutions are numerically accurate, as the results closely matched previous studies, ensuring reliability of the developed code.
- Skin friction decreases with higher M, λ and A_1 with β_1 strongly reducing and β_2 mildly reducing it the Nusselt number rises with β_3, Nr, $\Pr$ & θ_w but falls with Nb, Nt, A^* & B^* the Sherwood number grows with Le, Nb, Cr & δ but declines with Nt & E overall, Maxwell fluid yields the most favorable transport rates, Jeffrey the least and Oldroyd-B lies between, reflecting their rheological differences

REFERENCES

1. B.Srisailam et al. Lecturer, Department of Humanities & Sciences (Mathematics), Government Polytechnic, Suryapet, Telangana, India, B. Srisailam, K. S. Reddy, G. Narender, and B. S. Malga, "Flow and Heat Transfer Analysis MHD Nanofluid due to Convective Stretching Sheet," IJST, vol. 15, no. 44, pp. 2393–2402, Nov. 2022, https://doi.org/10.17485/IJST/v15i44.1006
2. Kapil kumar et al. "Heat and Mass transfer effect in Stagnation point flow of MHD Jeffery Nanofluid Flow over Porous Stretching sheet with Thermal Radiation," Int. J. Thin. Fil. Sci. Tec., vol. 13, no. 1, pp. 47–58, Jan. 2024, https://doi.org/10.18576/ijtfst/130106.
3. K.A.Khan et al., "Exploring the numerical simulation of Maxwell nanofluid flow over a stretching sheet with the influence of chemical reactions and thermal radiation," Results in Physics, vol. 60, p. 107635, May 2024, https://doi.org/10.1016/j.rinp.2024.107635.
4. S.Karthik, D.Iranian, H. Alhazmi, I. Khan, and A. Singh, "Heat transfer due to electromagnetic radiation of MHD Powell-Eyring fluid with mass diffusion via Lie symmetry scaling," Case Studies in Thermal Engineering, vol. 58, p. 104348, Jun. 2024, https://doi.org/10.1016/j.csite.2024.104348.
5. N.Sandeep and C.Sulochana, "Momentum and heat transfer behaviour of Jeffrey, Maxwell and Oldroyd-B nanofluids past a stretching surface with non-uniform heat source/sink," Ain Shams Engineering Journal, vol. 9, no. 4, pp. 517–524, Dec. 2018, https://doi.org/10.1016/j.asej.2016.02.008.
6. M.Almakki, S.K.Nandy, S.Mondal, P.Sibanda, and D.Sibanda, "A model for entropy generation in stagnation-point flow of non-Newtonian Jeffrey, Maxwell, and Oldroyd-B nanofluids," Heat Trans. Asian Res., vol. 48, no. 1, pp. 24–41, Jan. 2019, https://doi.org/10.1002/htj.21366.

7. A.S.Khan, Y.Nie, and Z.Shah, "Impact of Thermal Radiation and Heat Source/Sink on MHD Time-Dependent Thin-Film Flow of Oldroyed-B, Maxwell, and Jeffry Fluids over a Stretching Surface," Processes, vol. 7, no. 4, p. 191, Apr. 2019, https://doi.org/10.3390/pr7040191.
8. P.B.Raafat and F.N.Ibrahim, "Entropy and heat transfer investigation of Casson–Maxwell, Casson–Jeffrey, and Casson–Oldroyd-B binary nanofluids in a parabolic trough solar collector: a comparative study," J Therm Anal Calorim, vol. 148, no. 10, pp. 4477–4493, May 2023, https://doi.org/10.1007/s10973-023-12003-9.
9. G.R.Machireddy, M.M.Praveena, N.G.Rudraswamy, and G.K.Kumar, "Impact of Cattaneo–Christov heat flux on hydromagnetic flow of non-Newtonian fluids filled with Darcy–Forchheimer porous medium," Waves in Random and Complex Media, vol. 34, no. 4, pp. 2425–2442, Jul. 2024, https://doi.org/10.1080/17455030.2021.1957178.
10. D.Thenmozhi, M.Eswara Rao, Rlv. Renuka Devi, Ch. Nagalakshmi, and Pd. Selvi, "Dynamics of heat transfer in complex fluid systems: Comparative analysis of Jeffrey, Williamson and Maxwell fluids with chemical reactions and mixed convection," International Journal of Thermofluids, vol. 24, p. 100896, Nov. 2024, https://doi.org/10.1016/j.ijft.2024.100896.
11. T.Hayat, M.W.A.Khan, A.Alsaedi, M. Ayub, and M. I. Khan, "Stretched flow of Oldroyd-B fluid with Cattaneo-Christov heat flux," Results in Physics, vol. 7, pp. 2470–2476, 2017, https://doi.org/10.1016/j.rinp.2017.06.050.
12. T.Hayat, F.Haider, T.Muhammad, and A. Alsaedi, "Darcy-Forchheimer flow with Cattaneo-Christov heat flux and homogeneous-heterogeneous reactions," PLoS ONE, vol. 12, no. 4, p. e0174938, Apr. 2017, https://doi.org/10.1371/journal.pone.0174938.
13. A.Shahid, M.M.Bhatti, O.A.Bég, and A.Kadir, "Numerical study of radiative Maxwell viscoelastic magnetized flow from a stretching permeable sheet with the Cattaneo–Christov heat flux model," Neural Comput&Applic, vol. 30, no. 11, pp. 3467–3478, Dec. 2018, https://doi.org/10.1007/s00521-017-2933-8.
14. B.M.Shankaralingappa, B.C.Prasannakumara, B.J.Gireesha, and I.E.Sarris, "The Impact of Cattaneo–Christov Double Diffusion on Oldroyd-B Fluid Flow over a Stretching Sheet with Thermophoretic Particle Deposition and Relaxation Chemical Reaction," Inventions, vol. 6, no. 4, p. 95, Nov. 2021, https://doi.org/10.3390/inventions6040095.
15. F.Shahzad et al., "Electromagnetic Control and Dynamics of Generalized Burgers' Nanoliquid Flow Containing Motile Microorganisms with Cattaneo–Christov Relations: Galerkin Finite Element Mechanism," Applied Sciences, vol. 12, no. 17, p. 8636, Aug. 2022, https://doi.org/10.3390/app12178636.
16. P.Sreedevi and P.Sudarsana Reddy, "Comparative Study of Convective Oldroyd-B Nanofluid and Hybrid Nanofluid Flow, Heat and Mass Transfer Analysis Over Stretching Sheet with Cattaneo-Christov Heat Flux Model," j nanofluids, vol. 13, no. 3, pp. 839–850, Jun. 2024, https://doi.org/10.1166/jon.2024.2168.
17. A.O.M.Sidahmed, F.Salah, and K.K.Viswanathan, "Impact of chemical reaction on the Cattaneo–Christov heat flux model for viscoelastic flow over an exponentially stretching sheet," Sci Rep, vol. 14, no. 1, p. 16025, Jul. 2024, https://doi.org/10.1038/s41598-024-65642-9.
18. P.Soni, K.Sharma, H.Berrehal, and K. Jat, "Effect of Cattaneo–Christov heat flux model and elastic deformation on Walters'B viscoelastic fluid flow with porosity," International Journal of Thermofluids, vol. 24, p. 100825, Nov. 2024, https://doi.org/10.1016/j.ijft.2024.100825.
19. R.Abdullah Mohamed, A.Mahmoud Aly, S.Elsayed Ahmed, and M.Sayed Soliman, "MHD Jeffrey NanoFluids Flow Over a Stretching Sheet Through a Porous Medium in Presence of Nonlinear Thermal Radiation and Heat Generation/Absorption," CNMST, vol. 8, no. 1, Feb. 2020, https://doi.org/10.22111/tpnms.2019.29314.1172.
20. P.Kaswan, M.Kumar, and M.Kumari, "Analysis of a bioconvection flow of magnetocross nanofluid containing gyrotactic microorganisms with activation energy using an artificial neural network scheme," Results in Engineering, vol. 17, p. 101015, Mar. 2023, https://doi.org/10.1016/j.rineng.2023.101015.
21. K.Mahalakshmi and P.S.R.Murty, "Influence of Arrhenius activation energy and thermal radiation on unsteady MHD hybrid nanofluid flow with inclined stretching sheet in the presence of Brownian motion, and thermophoresis," Multiscale and Multidiscip. Model. Exp. and Des., vol. 8, no. 5, p. 240, May 2025, https://doi.org/10.1007/s41939-025-00815-1.
22. S.Bilal, S.U.Mamatha, C.S.K.Raju, B. Madhusudhana Rao, M. Y. Malik, and A. Akgül, "Dynamics of chemically reactive Jeffery fluid embedded in permeable media along with influence of magnetic field on associated boundary layers under multiple slip conditions," Results in Physics, vol. 28, p. 104558, Sep. 2021, https://doi.org/10.1016/j.rinp.2021.104558.
23. S.Jagadha et al., "Darcy Forchheimer two-dimensional thin flow of Jeffrey nanofluid with heat generation/absorption and thermal radiation over a stretchable flat sheet," Archives of Thermodynamics, pp. 247–259, May 2024, https://doi.org/10.24425/ather.2024.150869.
24. F.Ahmed et al., "Numerical modeling of a MHD non-linear radiative Maxwell nano fluid with activation energy," Heliyon, vol. 10, no. 2, p. e24098, Jan. 2024, https://doi.org/10.1016/j.heliyon.2024.e24098.
25. Y.Leng et al., "Computational study of magnetized and dual stratified effects on Non-Darcy Casson nanofluid flow: An activation energy analysis," Case Studies in Thermal Engineering, vol. 53, p. 103804, Jan. 2024, https://doi.org/10.1016/j.csite.2023.103804.
26. S.A.A.Shah et al., "Comparative study of some non-Newtonian nanofluid models across stretching sheet: a case of linear radiation and activation energy effects," Sci Rep, vol. 14, no. 1, p. 4950, Feb. 2024, https://doi.org/10.1038/s41598-024-54398-x.

27. S.J.Tao, F.Haq, A.Hussain, A.Shokri, M. R. Ali, and A. S. Hendy, "Computational framework for thermal transportation in radiative bio-convective micropolar nanomaterial flow over stretched sheet with entropy optimization," Case Studies in Thermal Engineering, vol. 59, p. 104549, Jul. 2024, https://doi.org/10.1016/j.csite.2024.104549.
28. K.Sudarmozhi et al., "Effect of heat generation and activation energy on MHD maxwell fluid with multiple slips," Case Studies in Thermal Engineering, vol. 59, p. 104424, Jul. 2024, https://doi.org/10.1016/j.csite.2024.104424.
29. M.V.Krishna and A. G. V. Kumar, "Chemical reaction, slip effects and non-linear thermal radiation on unsteady MHD Jeffreys nanofluid flow over a stretching sheet," Case Studies in Thermal Engineering, vol. 55, p. 104129, Mar. 2024, https://doi.org/10.1016/j.csite.2024.104129.
30. P.Rana and R. Bhargava, "Flow and heat transfer of a nanofluid over a nonlinearly stretching sheet: A numerical study," Communications in Nonlinear Science and Numerical Simulation, vol. 17, no. 1, pp. 212–226, Jan. 2012, https://doi.org/10.1016/j.cnsns.2011.05.009.
31. S.A.Lone, S.Anwar, A.Saeed, and G.Bognár, "A stratified flow of a non-Newtonian Casson fluid comprising microorganisms on a stretching sheet with activation energy," Sci Rep, vol. 13, no. 1, p. 11240, Jul. 2023, https://doi.org/10.1038/s41598-023-38260-0.
32. C.Sulochana, A.L.Nandeppanavar, M.M.Nandeppanavar, and M.Belagumpi, "Effect of activation energy and nonlinear thermal radiation on flow, heat and mass transfer of magneto-bioconvective Eyring–Powell nanofluid due to a stretching sheet," Proceedings of the Institution of Mechanical Engineers, Part N: Journal of Nanomaterials, Nanoengineering and Nanosystems, p. 23977914251330675, May 2025, https://doi.org/10.1177/23977914251330675.